Tracking and interception of ground-based RF sources using autonomous guided munitions with passive bearings-only sensors and tracking algorithms

Kenan Ezal* and Craig Agate
Toyon Research Corporation, 75 Aero Camino, Suite A, Goleta, CA, USA 93117

ABSTRACT

This paper considers the problem of tracking and intercepting a potentially moving ground-based RF source with an autonomous guided munition that has a passive bearings-only sensor located on its nose. It is assumed that the munition has lost GPS signal lock and that it relies only on its noisy inertial measurement unit (IMU) for guidance and navigation. Bearings-only target motion analysis (TMA) algorithms are used to obtain a position and velocity estimate for the RF source using the position, velocity and attitude estimates of the munition as well as the azimuth and elevation measurements obtained from the bearings-only RF sensor. Six degree-of-freedom (6-DOF) and three degree-of-freedom (3-DOF) munition models are used to evaluate the tracking and intercept/seeker performance of a hybrid coordinate (HC) extended Kalman filter (EKF), a particle filter (PF), a multiple hypothesis (MH) HC-EKF, and a pseudo-linear least squares (PLLS) filter.

Keywords: bearings-only, target motion analysis, guided munitions, RF seeker, location estimation, tracking, Kalman filter, pseudo-linear least squares filter, passive RF sensor

1. INTRODUCTION

Civilian and military navigation systems are increasingly relying on the accuracy of the information provided by the Global Positioning System (GPS). Moreover, since GPS receivers are now embedded in many different types of systems, this dependence goes far beyond inertial navigation and guidance systems and extends into areas such as personal communication systems (PCS) and wireless internet access systems. In military systems, the loss of GPS signal lock could cause an otherwise successful mission to become a failure, thus wasting valuable resources. In some cases, it could even mean the difference between life and death. The same is true in civilian applications. Therefore, it becomes imperative not only to protect the integrity of the GPS signal, but to locate and to eliminate any threats to GPS as soon as possible.

Although GPS has some built-in anti-jam (AJ) capabilities, it can be further augmented by integrating a GPS receiver with an Inertial Navigation System (INS) and by utilizing AJ GPS antennas. The performance of GPS/INS systems is especially crucial for guided missiles with extended ranges. Depending on the variant, the standoff range of unpowered guided missile systems can be as much as 100 kilometers. When a guided missile is tasked to fly deep behind enemy lines one should expect jammers to be placed anywhere along its trajectory, thereby increasing the probability of losing GPS signal lock sometime during the mission. If the flight time of an unpowered weapon is more than 100 seconds it is in danger of not achieving its accuracy requirements due to the potential loss of GPS signal lock somewhere along its trajectory. This is because once GPS signal lock has been lost, navigation errors grow at a rate which depends on the quality of the INS. A one degree-per-hour INS will have about a 30 meter circular error probable (CEP), that is, the radius which encloses 50% of all samples, within 100 seconds [1, 2]. This situation creates a dilemma for mission planners. That is, what is the weapon to do if it has lost GPS lock and is still too far away from its target to meet its accuracy requirements? One solution is to equip the munition with an angle-of-arrival (AOA) sensor that can provide the mission planner with a number of new opportunities in the event that GPS signal lock is lost. First, if so desired, it provides the missile with a jammer homing system. This is especially useful if the missile determines that the jammer and the designated target are collocated. In which case, it will permit the weapon to successfully complete its mission with potentially improved accuracy. Second, by sharing this information with other cooperative missiles and/or a central command, it will improve the success probability of future follow-on missions. Finally, the angle-of-arrival and power

* kezal@toyon.com; phone 1 805 968 6787 x180; fax 1 805 685 8089; www.toyon.com

Report Documentation Page

Form Approved
OMB No. 0704-0188

1. REPORT DATE	2. REPORT TYPE	3. DATES COVERED
2006		**00-00-2006 to 00-00-2006**

4. TITLE AND SUBTITLE	5a. CONTRACT NUMBER
Tracking and interception of ground-based RF sources using autonomous guided munitions with passive bearings-only sensors and tracking algorithms	5b. GRANT NUMBER
	5c. PROGRAM ELEMENT NUMBER
6. AUTHOR(S)	5d. PROJECT NUMBER
	5e. TASK NUMBER
	5f. WORK UNIT NUMBER
7. PERFORMING ORGANIZATION NAME(S) AND ADDRESS(ES) **Toyon Research Corporation,75 Aero Camino Suite A,Goleta,CA,93117**	8. PERFORMING ORGANIZATION REPORT NUMBER
9. SPONSORING/MONITORING AGENCY NAME(S) AND ADDRESS(ES)	10. SPONSOR/MONITOR'S ACRONYM(S)
	11. SPONSOR/MONITOR'S REPORT NUMBER(S)

12. DISTRIBUTION/AVAILABILITY STATEMENT
Approved for public release; distribution unlimited

13. SUPPLEMENTARY NOTES
The original document contains color images.

14. ABSTRACT
see report

15. SUBJECT TERMS

16. SECURITY CLASSIFICATION OF:			17. LIMITATION OF ABSTRACT	18. NUMBER OF PAGES	19a. NAME OF RESPONSIBLE PERSON
a. REPORT	b. ABSTRACT	c. THIS PAGE			
unclassified	**unclassified**	**unclassified**		**12**	

level information obtained from multiple missiles within a common area-of-interest can be fused together to improve our battlefield and situational awareness. With this added knowledge it will be possible to compute trajectories which could take advantage of regions of lower jamming power levels to reach designated targets. Power levels recorded by prior missions can also be used to determine the locations of large jamming sources, thus providing the location of new potential targets.

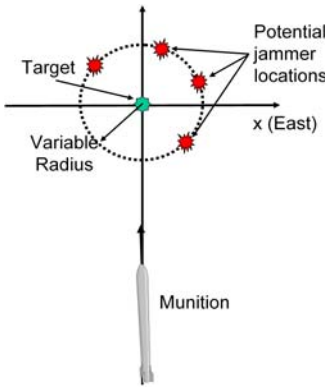

Figure 1: Scenario geometry

We are primarily interested in evaluating the performance of bearings-only target motion analysis (TMA) algorithms that use munition-based AOA sensor measurements as a means of tracking and homing on GPS jammers. The bearings-only tracking problem is also known as a passive tracking problem due to the fact that active radar is not utilized to obtain measurements of the target's motion. Typically, the measurements are the bearing angles in the direction of the target emissions in the form of elevation (θ) and azimuth (ϕ) angles. The emissions may be any form of RF emissions such as communication signals and radar or, perhaps, sonar signals emanating from the target.

Bearings-only TMA is a difficult problem to address because it has inherent observability issues [3, 4, 5] and the system equations have nonlinear components making it difficult to construct stable and unbiased estimators. In the standard extended Kalman filter (EKF) approach to this nonlinear problem the target state is defined in Cartesian coordinates so that the propagation of the state (i.e. the dynamic equation) is linear, while the nonlinear measurement equation is linearized through a Taylor series expansion. The Cartesian coordinate EKF (CC-EKF) is known to have divergence issues for the bearings-only problem, particularly when the target initialization is poor [3]. A particular variation of the CC-EKF is the Modified-Gain EKF (MG-EKF) of Song and Speyer [6] which, in our implementation, had similar divergence issues. Another algorithm, dubbed the pseudo-linear least-squares (PLLS), is obtained through some manipulation of the measurement equation and has very good convergence properties for stationary targets (Aidala, Nardone) [7]. However, the PLLS does lead to a biased estimator [8]. In this algorithm the set of pseudo-linear measurements are linear in the Cartesian state. The PLLS measurement matrix is a function of the range to the target and includes noise which ultimately leads to a bias in the state estimates.

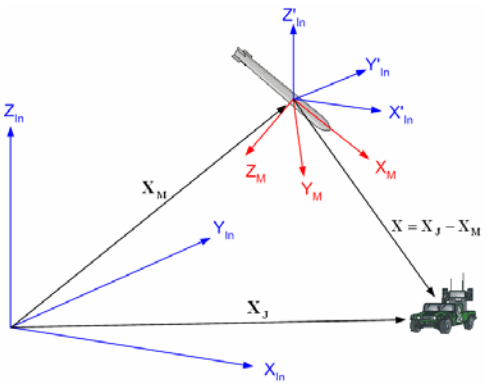

Figure 2: Coordinate system

Another variation of the EKF is the Modified Polar Coordinate EKF (MP-EKF) where the state dynamics are nonlinear and the measurement equation is linear [9]. The primary drawback to the MP-EKF approach is the complexity of the nonlinear state equation which requires an approximation for the state estimate. In contrast, the hybrid coordinate EKF (HC-EKF) is based on the observation that the state dynamics are linear in Cartesian coordinates while the measurement equation is linear in modified-polar coordinates [10, 11]. The approach is then to implement the Kalman filter equations in the coordinate system for which the process is linear. Thus, for propagation of the state estimate and error covariance matrix, the Kalman filter equations are implemented in Cartesian coordinates, and for state and covariance updating, the Kalman filter equations are implemented in modified-polar coordinates. The transformation of the state estimate from one coordinate system to the other is an exact mathematical process; whereas transforming the covariance requires an approximation. We found that the HC-EKF preserves the stability of the MP-EKF formulation while retaining the simplicity of the CC-EKF. Recent research has attempted to improve the performance of the CC-EKF by considering multiple initial conditions using parallel Kalman filters and weighting the outcome of

Error Parameter	Specification (1-sigma)
Gyro	
Bias	1 deg/hr
Scale Factor	150 ppm
Misalignment	100 mrad
Random Walk	0.1 deg/root hr
Accelerometer	
Bias	1 mg
Scale Factor	300 ppm
Misalignment	100 mrad

Figure 3: INS error model

each filter to come up with a single estimate [12, 13]. We implemented the multiple-hypothesis approach with the HC-EKF but did not see any improvement in performance. This was mostly likely due to the fact that the HC-EKF is inherently stable and has good convergence properties. Another family of filtering algorithms which has gained much interest in the last decade is the group of algorithms referred to as particle filters [14]. Particle filters are based on Monte Carlo simulation methods. One advantage of particle filters is that there is no assumption of linearity or Gaussian noise processes. The probability density function (PDF) of the jammer is approximated with points (the particles) in the state space. As the number of points representing the PDF increases, the computational expense associated with the algorithm increases as well.

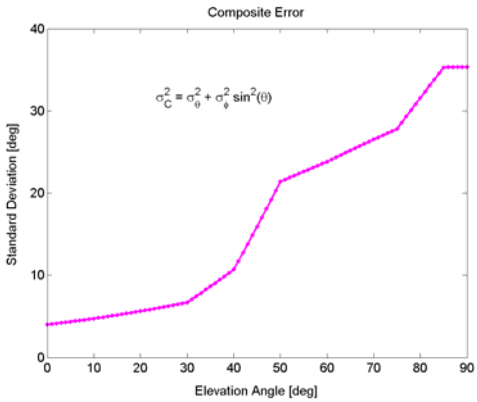

Figure 4: Angle error model

In this paper we consider a simple guided munition scenario with an AOA sensor on the nose of the munition. The scenario is described in the following section. We also limit ourselves to the discussion of the relative performance of the PLLS algorithm, the HC-EKF, the multiple-hypothesis HC-EKF (MH-HC-EKF), and the particle filter (PF) implementation. These algorithms are briefly described in Section 3. We provide some typical simulation results in Section 4 and concluding remarks in Section 5.

2. SCENARIO DESCRIPTION AND ASSUMPTIONS

A bird's eye view of the guided munition scenario is shown in **Figure 1**. A flat earth model is used with an east-north-up (ENU) inertial coordinate system. The sensor/munition coordinate system is defined in **Figure 2** with its x-axis going forward through the nose of the munition. The inertial position of the guided munition is denoted by $\mathbf{x}_M(t) \in R^3$. The intended target is at the origin and the jammer inertial position is denoted by $\mathbf{x}_J(t) \in R^3$. It is assumed that the jammer is traveling with a constant velocity $\dot{\mathbf{x}}(t) = \mathbf{v}_J$. Our simulation uses two different models for the missile dynamics. Both models attempt to capture the missile dynamics of an extended range munition and the navigation errors of both models are the same. The INS error model is shown in **Figure 3**. The first missile model is a 3-DOF dynamic model that computes the axial and normal aerodynamic forces acting on the body of the munition through a set of look-up tables that are a function of the Mach number and the angle of attack of the weapon. A piecewise exponential atmospheric density model is employed. Attitude error is modeled by adding rotational errors that are consistent with the INS error model of **Figure 3**. The second model is a full-blown 6-DOF dynamic model obtained from the Air Force using the VisSim™ environment by Visual Solutions Corporation.

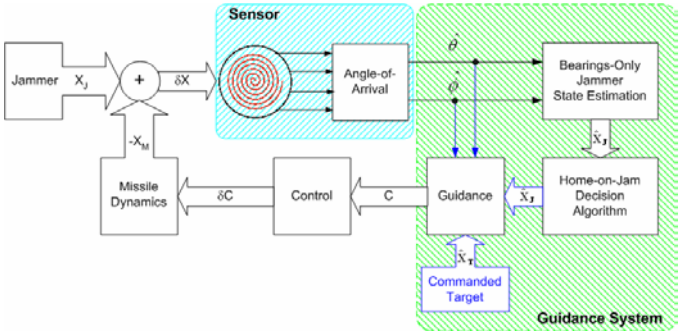

Figure 5: Simulation block diagram

The munition is released at time $t = T_L < 0$ and loses GPS signal lock at time $t = 0$. We are primarily interested in the period of time after GPS signal lock has been lost. Once GPS signal lock has been lost the weapon can do one of two things: it can continue to fly towards its intended target or it can home on the jammer. At $t = 0$ the munition begins to utilize the AOA sensor located on the nose of the weapon. The sensor measures the elevation angle (θ) and azimuth angle (ϕ) of the jammer relative to the munition in the sensor/munition coordinate system. Bearing measurements are taken every 10ms and these samples are averaged every 100ms. The elevation angle dependent Gaussian sensor noise model used in our simulations is represented in **Figure 4** by the composite angle error $\sigma_c^2 = \sigma_\theta^2 + \sin^2(\theta)\,\sigma_\phi^2$ where $E\{n_\theta\} = E\{n_\phi\} = 0$ and $E\{n_\theta^2\} = E\{n_\phi^2\} = \sigma_\theta^2 = \sigma_\phi^2$. The equation relating these angle measurements is given by

$$\begin{bmatrix}\phi_m(t)\\ \theta_m(t)\end{bmatrix}=\begin{bmatrix}\arctan\left(\tilde{r}_z(t)/\tilde{r}_y(t)\right)\\ \arctan\left(\sqrt{\tilde{r}_y^2(t)+\tilde{r}_z^2(t)}\,/\tilde{r}_x(t)\right)\end{bmatrix}+\begin{bmatrix}n_\phi(t)\\ n_\theta(t)\end{bmatrix} \qquad \textbf{(SCME)}$$

where $\tilde{\mathbf{r}}(k)\in R^3$ is the unit bearing vector in the direction of the jammer defined in the sensor/munition coordinate system.

The bearing measurements are used to compute an estimate of the jammer location using bearings-only localization algorithms. Selected algorithms are described in Section 3. The estimated jammer location and our confidence in the estimate are used to determine whether or not the munition will home on the jammer or continue toward its intended target. The decision algorithm itself is outside the scope of this paper and is not discussed. **Figure 5** shows the block diagram of the simulation components.

3. ALGORITHM DESCRIPTIONS

The state $\mathbf{x}_C=\begin{bmatrix}\mathbf{x}_J-\mathbf{x}_M\\ \dot{\mathbf{x}}_J-\dot{\mathbf{x}}_M\end{bmatrix}=\begin{bmatrix}\mathbf{R}\\ \dot{\mathbf{R}}\end{bmatrix}=\begin{bmatrix}\mathbf{x}_{C_1}\\ \mathbf{x}_{C_2}\end{bmatrix}\in R^6$ represents the position and velocity of the jammer relative to the weapon in Cartesian coordinates. Hence, $\dot{\mathbf{x}}_C=\frac{d}{dt}\mathbf{x}_C=\begin{bmatrix}\dot{\mathbf{R}}\\ \ddot{\mathbf{R}}\end{bmatrix}=\begin{bmatrix}\dot{\mathbf{R}}\\ \mathbf{a}_J-\mathbf{a}_0\end{bmatrix}$ where $\mathbf{a}_J$ represents the acceleration of the jammer, and $\mathbf{a}_0$ represents the acceleration of the weapon (i.e. sensor platform) which is assumed to be measured by the INS. We can put the above equation in matrix-vector form as

$$\dot{\mathbf{x}}_C=\begin{bmatrix}\mathbf{0}_{3x3} & \mathbf{I}_3\\ \mathbf{0}_{3x3} & \mathbf{0}_{3x3}\end{bmatrix}\begin{bmatrix}\mathbf{R}\\ \dot{\mathbf{R}}\end{bmatrix}+\begin{bmatrix}\mathbf{0}_{3x3}\\ \mathbf{I}_3\end{bmatrix}[\mathbf{a}_J-\mathbf{a}_0]$$

where $\mathbf{I}_3$ is the three by three identity matrix and $\mathbf{0}_{3x3}$ is the three by three zero matrix. Since the propagation is done in discrete time steps, the above equation can be discretized by integrating over one time step (T). Furthermore, we have assumed that the jammer is not accelerating, so that $\mathbf{a}_J\approx\mathbf{0}$. The resulting discrete-time equation modeling the system dynamics is given by

$$\begin{bmatrix}\mathbf{R}(k+1)\\ \dot{\mathbf{R}}(k+1)\end{bmatrix}=\begin{bmatrix}\mathbf{I}_3 & T\mathbf{I}_3\\ \mathbf{0}_{3x3} & \mathbf{I}_3\end{bmatrix}\begin{bmatrix}\mathbf{R}(k)\\ \dot{\mathbf{R}}(k)\end{bmatrix}+\begin{bmatrix}-\frac{T^2}{2}\mathbf{I}_3\\ -T\mathbf{I}_3\end{bmatrix}\mathbf{a}_0(k)\ \text{ or, equivalently, }\ \mathbf{x}_C(k+1)=\mathbf{\Phi}_k\mathbf{x}_C(k)+\mathbf{\Gamma}_k\mathbf{u}(k).$$

Our goal is to estimate the position of the jammer through an estimate of the range: $\hat{\mathbf{x}}_J=\hat{\mathbf{x}}_M+\hat{\mathbf{R}}$. An estimate of the missile position, $\hat{\mathbf{x}}_M$, is available from the INS.

The measurement equation (**CCME**) can be rewritten as

$$\mathbf{z}_C(k)=\begin{bmatrix}\phi_m(k)\\ \theta_m(k)\end{bmatrix}=\mathbf{f}(\mathbf{\Lambda}(k)\mathbf{r}(k))+\mathbf{n}(k) \qquad \textbf{(CCME)}$$

where $\mathbf{\Lambda}(k)\in R^{3x3}$ is a rotation matrix which transforms the unit bearing vector in the inertial coordinate system $\mathbf{r}(k)\in R^3$ to the unit bearing vector in the antenna coordinate system $\tilde{\mathbf{r}}(k)$. Since $\mathbf{f}(\bullet)$ is a nonlinear function, and $\mathbf{r}(k)=\mathbf{R}(k)/|\mathbf{R}(k)|$, the measurement equation (**CCME**) is a nonlinear function of the state $\mathbf{x}_C$. Hence, it is difficult to obtain an estimate of the state without some form of approximation. In fact, it has been demonstrated that the extended Kalman filter in Cartesian coordinates, which uses a Taylor approximation of (**CCME**), can lead to instabilities in the estimation process [3]. Selected alternative bearings-only estimation algorithms are described in the following sections.

3.1 Pseudo-Linear Least Squares (PLLS) Algorithm

In its simplest incarnation, the PLLS algorithm assumes that the jammer is stationary, that is $\dot{\mathbf{x}}_J = 0$. Since the jammer is assumed to be stationary, there are no dynamics to update and the observations are assumed to be pseudo-linear. While this filter is very simple to implement and remains stable, it is a biased estimator [8]. The filter is derived by defining bearing measurements in inertial coordinates. $\beta_{x/z}(k) = \arctan\left(\mathbf{R}_X(k)/\mathbf{R}_Z(k)\right) = \arctan\left(\mathbf{r}_X(k)/\mathbf{r}_Z(k)\right)$ with $\beta_{y/x}(k)$ and $\beta_{z/y}(k)$ defined in a similar manner and where

$$\begin{bmatrix} \mathbf{x}_{J_X}(k) - \mathbf{x}_{M_X}(k) \\ \mathbf{x}_{J_Y}(k) - \mathbf{x}_{M_Y}(k) \\ \mathbf{x}_{J_Z}(k) - \mathbf{x}_{M_Z}(k) \end{bmatrix} = \begin{bmatrix} \mathbf{R}_X(k) \\ \mathbf{R}_Y(k) \\ \mathbf{R}_Z(k) \end{bmatrix} = \left|\mathbf{R}(k)\right| \begin{bmatrix} \mathbf{r}_X(k) \\ \mathbf{r}_Y(k) \\ \mathbf{r}_Z(k) \end{bmatrix} = \left|\mathbf{R}(k)\right| \mathbf{\Lambda}^T(k)\tilde{\mathbf{r}}(k).$$

Assuming an additive Gaussian noise,

$$\begin{bmatrix} \beta_{x/z}(k) \\ \beta_{y/x}(k) \\ \beta_{z/y}(k) \end{bmatrix} = \begin{bmatrix} \arctan\left(\mathbf{R}_X(k)/\mathbf{R}_Z(k)\right) \\ \arctan\left(\mathbf{R}_Y(k)/\mathbf{R}_X(k)\right) \\ \arctan\left(\mathbf{R}_Z(k)/\mathbf{R}_Y(k)\right) \end{bmatrix} + \begin{bmatrix} \mathbf{n}_{x/z}(k) \\ \mathbf{n}_{y/x}(k) \\ \mathbf{n}_{z/y}(k) \end{bmatrix} = \begin{bmatrix} \arctan\left(\mathbf{r}_X(k)/\mathbf{r}_Z(k)\right) \\ \arctan\left(\mathbf{r}_Y(k)/\mathbf{r}_X(k)\right) \\ \arctan\left(\mathbf{r}_Z(k)/\mathbf{r}_Y(k)\right) \end{bmatrix} + \mathbf{n}(k), \text{ with } \cos(\mathbf{n}(k)) \approx \mathbf{1},$$

and defining $\overline{\mathbf{R}}_{x/z}(k) = \sqrt{\mathbf{r}_X^2(k) + \mathbf{r}_Z^2(k)}$, $\overline{\mathbf{R}}_{y/x}(k) = \sqrt{\mathbf{r}_x^2(k) + \mathbf{r}_y^2(k)}$, $\overline{\mathbf{R}}_{z/y}(k) = \sqrt{\mathbf{r}_Y^2(k) + \mathbf{r}_Z^2(k)}$,

$$\mathbf{n}_P(k) = \left|\mathbf{R}(k)\right| \begin{bmatrix} \overline{\mathbf{R}}_{x/z}(k)\sin(\mathbf{n}_{x/z}(k)) \\ \overline{\mathbf{R}}_{y/x}(k)\sin(\mathbf{n}_{y/x}(k)) \\ \overline{\mathbf{R}}_{z/y}(k)\sin(\mathbf{n}_{z/y}(k)) \end{bmatrix}, \text{ and } \mathbf{H}(k) = \begin{bmatrix} -\cos(\beta_{x/z}(k)) & \sin(\beta_{y/x}(k)) & 0 \\ 0 & -\cos(\beta_{y/x}) & \sin(\beta_{z/y}(k)) \\ \sin(\beta_{x/z}(k)) & 0 & -\cos(\beta_{z/y}(k)) \end{bmatrix},$$

we can write the measurement equation as a linear function of the inertial state of the jammer and the munition:

$$\mathbf{z}_P(k) = \mathbf{H}^T(k)\mathbf{x}_M = \mathbf{H}^T(k)\mathbf{x}_J - \mathbf{n}_P(k). \qquad \textbf{(PLME)}$$

We note that $\mathbf{z}_P(k) = \mathbf{H}^T(k)\mathbf{x}_M$ is a measured quantity since it is a function of the (noisy) bearing angles in inertial coordinates. The term $\mathbf{n}_P(k)$ is the effective noise of the system. The measurement equation (**PLME**) can now be directly applied to the standard least-squares recursive form:

$$\begin{aligned} \mathbf{K}(k) &= \mathbf{P}(k-1)\mathbf{H}(k)\left[\mathbf{I} + \mathbf{H}^T(k)\mathbf{P}(k-1)\mathbf{H}(k)\right]^{-1} \\ \hat{\mathbf{x}}_J(k) &= \hat{\mathbf{x}}_J(k-1) + \mathbf{K}(k)\left[\mathbf{z}_P(k) - \mathbf{H}^T(k)\hat{\mathbf{x}}_J(k-1)\right] \\ \mathbf{P}(k) &= \mathbf{P}(k-1) - \mathbf{K}(k)\mathbf{H}^T(k)\mathbf{P}(k-1) \end{aligned} \qquad \textbf{(PLLS)}$$

where $\hat{\mathbf{x}}_J(0) = \mathbf{x}_0$ is the initial estimate of the jammer location and $\mathbf{P}(0) = \lambda\mathbf{I} > 0$ for any positive constant λ.

In our simulations, the covariance $\mathbf{P}$ is reset every 5 seconds with $\lambda = 0.02$, and $\mathbf{x}_0$ is initialized after 4 seconds of filtered bearing measurements have been accumulated. The filtered bearing measurements are extrapolated to intersect ground level (defined as the target altitude) to determine the initial position estimate. The separation angle between the latest LOS vector to the jammer position estimate is continuously monitored. The filter is reinitialized if the separation angle exceeds five degrees. The new initial condition is selected along the latest measured LOS vector at a range equal to the last position estimate range.

3.2 Hybrid Coordinate Extended Kalman Filter (HC-EKF)

The HC-EKF is based on the observation that the measurement equation is linear in modified-polar coordinates while the state dynamics are linear in Cartesian coordinates. The approach is then to implement the Kalman filter equations in

the coordinate system for which the process is linear. The jammer state in modified-polar coordinates $\mathbf{x}_{MP} = \left[\mathbf{r}^T \quad \dot{\mathbf{r}}^T \quad |\mathbf{R}|^{-1} \quad \left(\left(d|\mathbf{R}|/dt\right)/|\mathbf{R}|\right)\right]^T \in R^8$ includes the unit line-of-sight (LOS) vector $\mathbf{x}_{MP_1} \equiv \mathbf{r} \in R^3$, the time-derivative of the unit LOS vector $\mathbf{x}_{MP_2} \equiv \dot{\mathbf{r}} \in R^3$, the inverse of the range $\mathbf{x}_{MP_3} \equiv |\mathbf{R}|^{-1} \in R$, and the range rate divided by the range $\mathbf{x}_{MP_4} \equiv \left(d|\mathbf{R}|/dt\right)/|\mathbf{R}| \in R$. In the standard hybrid-coordinate EKF implementation, the measurement is a direction cosine vector in the direction of the jammer and, hence, the measurement equation in modified-polar coordinates is a linear function of the state [10, 11]:

$$\mathbf{z}_{MP}(k) = \mathbf{\Lambda}_{3x3}(k)\mathbf{r}(k) + \mathbf{n}(k) = \left[\mathbf{\Lambda}_{3x3}(k) \quad \mathbf{0}_{3x3} \quad 0 \quad 0\right]\mathbf{x}_{MP}(k) + \mathbf{n}(k). \qquad \textbf{(MPME)}$$

Thus, for propagation of the state estimate and error covariance matrix, the Kalman filter equations are implemented in Cartesian coordinates, and for state and covariance updating, the Kalman filter equations are implemented in modified-polar coordinates. The transformation of the state estimate from one coordinate system to the other is an exact mathematical process whereas transforming the covariance requires a Jacobian and, hence, an approximation.

In our implementation, we note that a unit vector in the direction of the measured LOS is equivalent to measuring the elevation and azimuth angles. If the measurement were the bearing vector and not the bearing angles, the resulting measurement equation would be linear in modified-polar coordinates. In fact, the measurement would be a noisy version of $\mathbf{x}_{MP_1}(k)$. Thus, we transform the measurements from bearing angles to a bearing vector representing a unit LOS vector to the jammer:

$$\mathbf{z}_H(k) = \begin{bmatrix} \cos(\theta_m(k)) \\ \sin(\theta_m(k))\cos(\phi_m(k)) \\ \sin(\theta_m(k))\sin(\phi_m(k)) \end{bmatrix} \approx \left[\mathbf{\Lambda}(k) \vdots \mathbf{0}_{3x5}\right]\mathbf{x}_{MP} + \mathbf{n}(k) = \tilde{\mathbf{r}}(k) + \mathbf{n}(k) = \mathbf{\Lambda}(k)\mathbf{r}(k) + \mathbf{n}(k) \qquad \textbf{(HCME)}$$

where $\mathbf{0}_{3x5}$ is the 3 by 5 zero matrix. Note that the equation above is an approximation since the noisy measured elevation, $\theta_m(k)$, is given by $\theta_m(k) = \theta(k) + n_\theta(k)$ where $\theta(k)$ is the *true* elevation angle. In order to use the Kalman filter update equation it is necessary to derive the approximate noise characteristics of $\mathbf{n}(k)$, or the measurement error covariance matrix. Hence, we must expand the sinusoidal functions and find the mean and variance of the "noise" term for each component of the measurement vector. For example, we expand the cosine function for the first component of $\mathbf{z}_H(k)$ as follows

$$z_1(k) = \cos(\theta(k))\cos(n_\theta(k)) - \sin(\theta(k))\sin(n_\theta(k))$$

where $n_\theta(k)$ is a zero-mean Gaussian random variable with a variance of σ_θ^2. Assuming that the magnitude of the noise is small, we approximate the cosine of the noise as one which yields

$$z_1(k) \approx \cos\left(\theta(k)\right) + n_1(k)$$

where $n_1(k) = \sin\left(\theta(k)\right)\sin\left(n_\theta(k)\right)$. It can be shown that the mean and variance of $n_1(k)$ are given by

$$E\left\{n_1(k)\right\} = 0$$
$$E\left\{n_1^2(k)\right\} \equiv \sigma_1^2(k) = \frac{1}{2}\sin^2\left(\theta(k)\right)\left[1 - e^{-2\sigma_\theta^2}\right]$$

In the same way, we can determine the noise statistics for $z_2(k)$ and $z_3(k)$:

$$z_2(k) = \sin\left(\theta_m(k)\right)\cos\left(\phi_m(k)\right) \approx \sin\left(\theta(k)\right)\cos\left(\phi(k)\right) + n_2(k)$$
$$z_3(k) = \sin\left(\theta_m(k)\right)\sin\left(\phi_m(k)\right) \approx \sin\left(\theta(k)\right)\sin\left(\phi(k)\right) + n_3(k)$$

The statistics on $n_2(k)$ and $n_3(k)$ are assumed Gaussian with

$$E\{n_2(k)\} = E\{n_3(k)\} = 0$$

$$E\{n_2^2(k)\} \equiv \sigma_2^2(k) = 0.25\cos^2(\theta(k))\cos^2(\phi(k))\left[1-e^{-2\sigma_\theta^2}\right]\left[1+e^{-2\sigma_\phi^2}\right]$$
$$+0.25\cos^2(\theta(k))\sin^2(\phi(k))\left[1-e^{-2\sigma_\theta^2}\right]\left[1-e^{-2\sigma_\phi^2}\right]+0.25\sin^2(\theta(k))\sin^2(\phi(k))\left[1+e^{-2\sigma_\theta^2}\right]\left[1-e^{-2\sigma_\phi^2}\right]$$

$$E\{n_3^2(k)\} \equiv \sigma_3^2(k) = 0.25\cos^2(\theta(k))\sin^2(\phi(k))\left[1-e^{-2\sigma_\theta^2}\right]\left[1+e^{-2\sigma_\phi^2}\right]$$
$$+0.25\sin^2(\theta(k))\cos^2(\phi(k))\left[1+e^{-2\sigma_\theta^2}\right]\left[1-e^{-2\sigma_\phi^2}\right]+0.25\cos^2(\theta(k))\cos^2(\phi(k))\left[1-e^{-2\sigma_\theta^2}\right]\left[1-e^{-2\sigma_\phi^2}\right]$$

We stress that the actual measurements are the elevation and azimuth angles representing the direction from which the jammer energy emanates. These measurements are transformed so that the measurement equation can be expressed as a linear function of the modified-polar state variables. Note that the variance on the angle estimates is a function of the actual angles. For example, the variance on the elevation angle estimate increases as the elevation angle increases. Thus, throughout the flight of the weapon, the accuracy of the angle of arrival estimates varies, and we want our measurement noise covariance to reflect this difference. Thus, the measurements are weighted according to their accuracy. By accounting for the true time-varying nature of the measurement error covariance matrix, we build a more robust algorithm.

The transformations between the Cartesian and modified-polar coordinate systems are derived in a straightforward manner; therefore, only the results will be given here (see [10 and 11] for more detail). The nonlinear vector function which transforms the state in modified-polar coordinates to the state in Cartesian coordinates is denoted $\mathbf{g}_{MP}^{C}(\mathbf{x}_{MP}): R^8 \to R^6$ and is given by

$$\mathbf{x}_C = \begin{bmatrix}\mathbf{R}\\ \dot{\mathbf{R}}\end{bmatrix} = \mathbf{g}_{MP}^{C}(\mathbf{x}_{MP}) = \begin{bmatrix} \dfrac{\mathbf{x}_{MP_1}}{x_{MP_3}} \\ \dfrac{\mathbf{x}_{MP_2}}{x_{MP_3}} + \dfrac{x_{MP_4}}{x_{MP_3}}\mathbf{x}_{MP_1} \end{bmatrix}$$

Likewise, the nonlinear vector function which transforms the state in Cartesian coordinates to the state in modified-polar coordinates is denoted $\mathbf{g}_{C}^{MP}(\mathbf{x}_C): R^6 \to R^8$ and is given by

$$\mathbf{x}_{MP} = \begin{bmatrix} \mathbf{r} \\ \dot{\mathbf{r}} \\ \dfrac{1}{|\mathbf{R}|} \\ \dfrac{1}{|\mathbf{R}|}\dfrac{d|\mathbf{R}|}{dt} \end{bmatrix} = \mathbf{g}_{C}^{MP}(\mathbf{x}_C) = \begin{bmatrix} \dfrac{\mathbf{x}_{C_1}}{|\mathbf{x}_{C_1}|} \\ \dfrac{1}{|\mathbf{x}_{C_1}|}\left(\mathbf{I}_3 - \dfrac{\mathbf{x}_{C_1}\mathbf{x}_{C_1}^T}{\mathbf{x}_{C_1}^T\mathbf{x}_{C_1}}\right)\mathbf{x}_{C_2} \\ \dfrac{1}{|\mathbf{x}_{C_1}|} \\ \dfrac{\mathbf{x}_{C_1}^T\mathbf{x}_{C_2}}{\mathbf{x}_{C_1}^T\mathbf{x}_{C_1}} \end{bmatrix}$$

The above equations exactly transform the state estimate from either coordinate system into the other system. What remains, then, is the transformation of the covariance matrices from one coordinate system to the other. It is this step

which introduces modeling errors and is only approximate. The transformation of the covariance matrix in Cartesian coordinates, $\mathbf{P}_C$, to that in modified-polar coordinates, $\mathbf{P}_{MP}$ is given by $\mathbf{P}_{MP} = \mathbf{J}_C^{MP}\mathbf{P}_C(\mathbf{J}_C^{MP})^T$ where $\mathbf{J}_C^{MP}$ is the Jacobian matrix of the transformation from Cartesian to modified-polar coordinates and is given by

$$\mathbf{J}_C^{MP}(\mathbf{x}_{MP}) = \begin{bmatrix} \dfrac{\left(\mathbf{I} - \mathbf{r}\mathbf{r}^T\right)}{|\mathbf{R}|} & \mathbf{0}_{3x3} \\ \mathbf{J}_{2,1} & \dfrac{\left(\mathbf{I} - \mathbf{r}\mathbf{r}^T\right)}{|\mathbf{R}|} \\ \dfrac{-\mathbf{r}^T}{|\mathbf{R}|^2} & \mathbf{0}_{1x3} \\ \mathbf{J}_{4,1} & \dfrac{\mathbf{r}^T}{|\mathbf{R}|} \end{bmatrix}$$

where $\mathbf{J}_{2,1} = -\dfrac{1}{|\mathbf{R}|}\left(\dot{\mathbf{r}}\mathbf{r}^T + \mathbf{r}\dot{\mathbf{r}}^T\right) - \dfrac{1}{|\mathbf{R}|^2}\dfrac{d|\mathbf{R}|}{dt}\left(\mathbf{I} - \mathbf{r}\mathbf{r}^T\right)$ and $\mathbf{J}_{4,1} = \dfrac{1}{|\mathbf{R}|}\left[\dot{\mathbf{r}}^T - \left(\dfrac{1}{|\mathbf{R}|}\dfrac{d|\mathbf{R}|}{dt}\right)\mathbf{r}^T\right]$. Finally, the Jacobian of the transformation from modified-polar to Cartesian coordinates is given by

$$\mathbf{J}_{MP}^C = \begin{bmatrix} |\mathbf{R}|\mathbf{I}_3 & \mathbf{0}_{3x3} & -|\mathbf{R}|^2\mathbf{r} & \mathbf{0}_{3x1} \\ \left(\dfrac{d|\mathbf{R}|}{dt}\right)\mathbf{I}_3 & |\mathbf{R}|\mathbf{I}_3 & \mathbf{J}_{2,3} & |\mathbf{R}|\mathbf{r} \end{bmatrix} \text{ where } \mathbf{J}_{2,3} = -|\mathbf{R}|^2\left[\dot{\mathbf{r}} + \left(\dfrac{1}{|\mathbf{R}|}\dfrac{d|\mathbf{R}|}{dt}\right)\mathbf{r}\right].$$

3.3 Multiple Hypothesis Hybrid Coordinate Extended Kalman Filter (MH-HC-EKF)

A common problem with applying the EKF to the bearings-only tracking problem is divergence of the filter. It is observed that this generally occurs with poor initialization. The range-parameterized algorithm simply runs several EKFs in parallel, each initialized differently [12, 13]. Typically, the jammer is known to lie in a certain region of the state space through prior information. The space in the direction of the LOS is chopped up into range bins and each filter is initialized using the mean of each range bin as the range to the target. Given the first bearing measurement, the initial estimate of the jammer position for each EKF is determined by this bearing and the mean value of the range bin for the corresponding EKF. Thus, multiple filters are estimating the position of the jammer, each initialized with a different value. Each filter's estimate can be considered as a hypothesis. The "probability" that each filter's estimate is the correct one is found using the value of the measurement likelihood. Note that this is somewhat ad-hoc in the sense that the hypotheses are not disjoint events. Another perspective on this approach is that we have several independent filters tracking the same object. The measurement likelihood is an indication of how well the filter's predicted measurement matches the actual measurement. Thus, the measurement likelihood is a confidence value on the accuracy of each filter's estimate. This confidence value is used to weight each filter estimate. The overall estimate is then the weighted sum of each filter estimate. The benefit over a single Kalman filter is that any of the filters which begin to diverge will exhibit this divergence in the measurement likelihood leading to low confidence values. Thus, these filters will contribute little to the overall estimate and, when subject to a pruning technique, will be discontinued.

There is certainly intuitive appeal to this multiple EKF approach. We implemented this for the hybrid algorithm but found the results to be worse than for a single hybrid filter. The reasoning is that the hybrid filter rarely diverges (we found no cases for which it did) and, thus, all parallel filters continue to track and converge to the correct estimate. However, depending on the initial estimate, the filters have different convergence rates, and the good estimates get diluted with the poor estimates. Perhaps for a standard EKF which is prone to divergence under poor initialization the range-parameterized algorithm will improve performance.

3.4 Particle Filter (PF)

The Bayesian framework for filtering problems represents a theoretically sound approach which entails determining the PDF of an unknown parameter. The following formula, referred to as Bayes' Rule, provides a means by which the prior PDF of some unknown random time-varying parameter $\mathbf{x}(k)$ is updated using a likelihood function

$$p(\mathbf{x}(k) \mid Y^k) = \frac{p(\mathbf{y}(k) \mid \mathbf{x}(k)) p(\mathbf{x}(k) \mid Y^{k-1})}{p(\mathbf{y}(k) \mid Y^{k-1})} \qquad \textbf{(BU)}$$

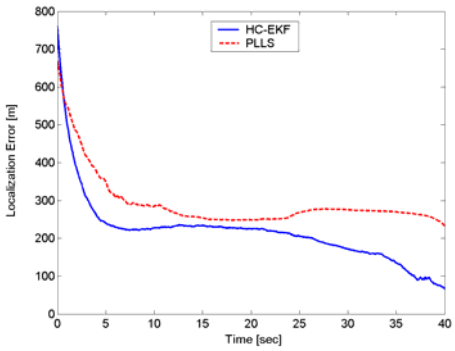

Figure 6: HC-EKF vs. PLLS with 3-DOF model and jammer at (-1, 0, 0) km

where $Y^k = \{\mathbf{y}(1), \mathbf{y}(2), ..., \mathbf{y}(k)\}$ represents a sequence of measurements. The measurements are related to the unknown parameter through the following measurement equation

$$\mathbf{y}(k) = \mathbf{h}_k(\mathbf{x}(k), \mathbf{v}(k)) \qquad \textbf{(NLME)}$$

where $\mathbf{h}_k(\cdot,\cdot)$ is a possibly time-varying nonlinear function of the unknown parameter $\mathbf{x}(k)$, and $\mathbf{v}(k)$ is typically assumed to be a sample of a white noise measurement process whose PDF is known. The state is assumed to evolve according to the following general dynamic equation

$$\mathbf{x}(k+1) = \mathbf{f}_k(\mathbf{x}(k), \mathbf{w}(k)) \qquad \textbf{(NLSE)}$$

where $f_k(\cdot,\cdot)$ may be a time-varying nonlinear function of the state and $\mathbf{w}(k)$ is typically modeled as a white noise process with a known PDF. The difficulty in analytically determining the PDF of $\mathbf{x}(k)$ is that only for special cases does a closed-form (i.e., finite) description of $p(\mathbf{x}(k) \mid Y^k)$ exist. When **(NLME)** and **(NLSE)** take on the special linear forms

$$\begin{aligned} \mathbf{x}(k+1) &= \mathbf{F}(k)\mathbf{x}(k) + \mathbf{\Gamma}(k)\mathbf{w}(k) \\ \mathbf{y}(k) &= \mathbf{H}(k)\mathbf{x}(k) + \mathbf{v}(k) \end{aligned} \qquad \textbf{(LE)}$$

where $\mathbf{w}(k)$ and $\mathbf{v}(k)$ are samples from a Gaussian white noise process, then the PDFs are all Gaussian and, thus, are completely characterized by the first and second moments (i.e., mean and covariance). For the linear case modeled as in **(LE)**, the resulting Bayes' implementation is the well-known Kalman Filter. However, for a plethora of other cases (e.g., nonlinear, non-Gaussian), the Kalman filter is inappropriate. While some success has been achieved by applying the EKF (Extended Kalman filter), derived by linearizing the measurement equation and/or dynamic equation, the behavior of the EKF is often unpredictable. The difficulty in applying the EKF lies in the underlying assumption that the PDF of the unknown parameter (i.e., target state) can be sufficiently approximated by a Gaussian density function, a dubious assumption, particularly for the case of multimodal PDFs.

When linearization of the measurement model and/or dynamic model is not feasible or leads to unsatisfactory results, another approach to the implementation of Bayes' methods is the approximation of the true PDF of $\mathbf{x}(k)$ using a model density. Various approximations include a piece-wise constant approximation, point-mass approximation or Gaussian sum approximation of the true posterior PDF of the target state. These "deterministic" methods all involve approximating the PDF of the state on a fixed grid over the state space and, therefore, suffer from the "curse of dimensionality." To cope with the computational complexity of these fixed-grid approaches, sub-optimal pruning of basis functions (i.e., points in the grid) is usually required. In contrast, the method described next naturally implements a randomly evolving grid based on the likelihoods of the received data.

Stochastic sampling methods randomly sample points in the state space and calculate the PDF at these points. Referred to generally as Monte Carlo methods, the computation required for their implementation in real-time systems precluded

them from use except in statistical batch processing type applications. With the revolution in computing power over the last decade and advent of parallel computing structures (particle filtering methods are easily parallelizable), Monte Carlo methods have experienced a resurgence in the field of estimation and filtering [14]. Particle filters (also referred to as weighted bootstrap filters) are based on the solution to the following problem, "Given samples from a PDF $g(x)$, can one generate samples of an arbitrary PDF, $f(x)$?" There are different methods by which this can be achieved, one of which is the weighted bootstrap method on which particle methods are based. For illustrative purposes we demonstrate the implementation of (**BU**), which is the "update" step in the Bayes' approach to filtering. Given that we have samples $\mathbf{x}_i(k)$, $i = 1,2,...,n,$ which were drawn from the predicted density, $p(\mathbf{x}(k) \mid Y^{k-1})$, the following procedure is used to simulate a set of samples drawn from $p(\mathbf{x}(k) \mid Y^k)$. First, after receiving a measurement, $\mathbf{y}(k)$, the weights

$$q_i = \frac{p(\mathbf{y}(k) \mid \mathbf{x}_i(k))}{\sum p(\mathbf{y}(k) \mid \mathbf{x}_j(k))} \qquad i = 1,2,3,...,n,$$

are calculated using the likelihood function evaluated at $\mathbf{y}(k)$. Next, a discrete distribution is formed over the samples $\mathbf{x}_i(k)$ with q_i as the weights. Finally, this discrete distribution is resampled n times yielding a set of points which simulate samples drawn from the density, $p(\mathbf{x}(k) \mid Y^k)$. The requirements for implementing the weighted bootstrap filtering algorithm are that a prior distribution on the unknown random parameter is available for sampling, the likelihoods are available and the PDF of $\mathbf{w}(k)$ in (**LE**) is available for sampling. Note the absence of reliance on linearity or Gaussian noise statistics. In fact, a closed-form expression for the likelihood function is not even necessary. It is sufficient that the likelihood be evaluated pointwise for any point in the state space. Thus, particle filtering methods are applicable to a much wider range of estimation problems than traditional linear Kalman Filters. Furthermore, there exists a justification [14] of the convergence of particle approximations to the true PDFs, results which are lacking for ad-hoc methods such as the EKF.

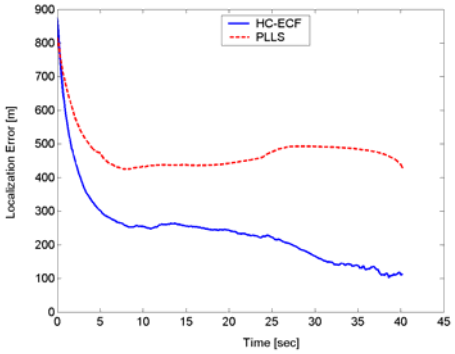

Figure 7: HC-EKF vs. PLLS with 3-DOF model and jammer at (-2, 0, 0) km

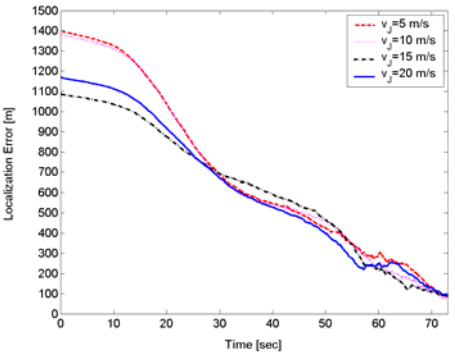

Figure 8: HC-EKF localization error with 6-DOF model and moving jammer

4. SIMULATION RESULTS

All four algorithms, the PLLS algorithm, the HC-EKF, the MH-HC-EKF, and the PF, were individually optimized for the simulation assumptions including measurement and process noise values. Each algorithm was run for varying flight times and conditions and with both 3-DOF and 6-DOF dynamic models. The scenario with the 3-DOF munition model was set up such that the munition lost GPS lock at (0, -8, 7.62) km while traveling due north at Mach 0.8. The unaided flight time is approximately 40 seconds. The 6-DOF scenario was set up such that the munition lost GPS lock at (0, -15, 7.62) km while flying due north at Mach 0.8. The unaided flight time was approximately 73 seconds. We found all four algorithms to be stable but we did verify the bias properties the PLLS filter. Essentially, the PLLS localization error was highly dependent on the system noise, the distance to the jammer,

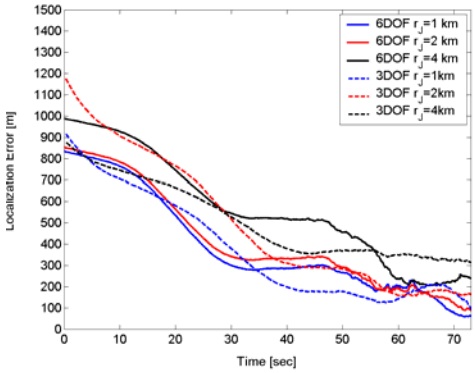

Figure 9: HC-EKF performance for 3-DOF and 6-DOF dynamic models

and the geometry. The performance of the PLLS algorithm was also degraded when the jammer was moving with a constant velocity. We now present results that are representative of the performance of each algorithm.

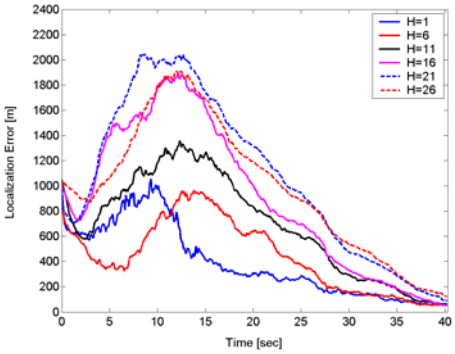

Figure 10: MH-HC-EKF for various numbers of parallel filters

Figure 6 shows the localization performance of the PLLS algorithm and the HC-EKF when the 3-DOF munition model is used and the stationary jammer is at (-1, 0, 0) km. We note that localization error in meters CEP for the HC-EKF was less than the error for the PLLS algorithm for the duration of the flight and is significantly lower at the end of the flight (< 100 m CEP vs.> 250 m CEP). The difference in the performance of the two algorithms was significantly more pronounced when the jammer was moved further away from the origin (the final destination of the munition.) **Figure 7** demonstrates this fact for the same initial conditions as the previous figure except that the jammer is now at (-2, 0, 0) km. The final localization error for the HC-EKF is ~100 m CEP while the localization error for the PLLS algorithm is greater than 400 m CEP.

Figure 8 shows the response of the HC-EKF when the jammer is moving with a constant velocity of $\left(v/\sqrt{2}, v/\sqrt{2}, 0\right)$ where v = 5, 10, 15, and 20 m/s. In this case the 6-DOF munition is utilized. The figure demonstrates that the final localization error for the HC-EKF is less than 100 m CEP for all cases. Although we have not included supporting data, the localization error for the HC-EKF also did not appear to depend on the range to the jammer, i.e., the HC-EKF appears to be unbiased with respect to range. **Figure 9** demonstrates that the filter performance did not significantly depend on the munition model employed. It shows the HC-EKF response for a stationary jammer located at (-r, 0, 0) for r = 1, 2, and 4 km. In this case the 3-DOF munition had the same initial conditions as the 6-DOF model with a 73 second unaided flight time.

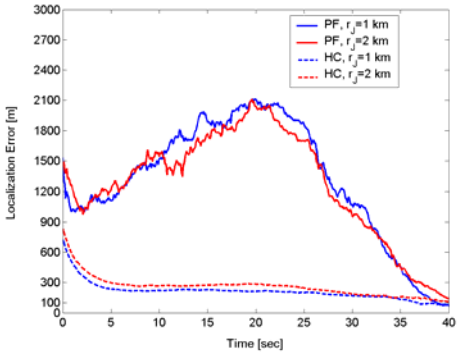

Figure 11: HC-EKF vs. PF filter performance

Figures **10** and **11** compare the performance of the HC-EKF to that of the MH-EC-EKF and the PF. In both cases the 3-DOF munition model is employed. In **Figure 10** we varied the number of initial hypothesis considered for the range-parameterized (multiple-hypothesis) HC-EKF. The figure shows the response of the algorithm for H = 1, 6, 11, 16, 21, and 26 where H is the number of parallel filters considered. It appears that a single HC-EKF (H = 1) is sufficient for good performance. **Figure 11** compares the performance of the HC-EKF with that of the PF. The figure demonstrates that while the final localization error of the PF is comparable under various different geometries to that of the HC-EKF (~ 100 m CEP), the HC-EKF is able to maintain a significantly lower localization error for a much greater portion of the trajectory.

Finally, **Figure 12**, shows typical impact errors for the case when the munition pursued the jammer instead of the intended target at the origin. While the impact errors of **Figure 12** were less than 1.7 m CEP, we found that the impact errors for various stationary jammer geometries and various unaided flight time durations were all within 2.5 m CEP for both the 3-DOF and 6-DOF munition models. The guidance laws for both the 3-DOF and 6-DOF munition models were based on classical proportional guidance. A commanded impact angle of 71° was always achieved. Only the PLLS and HC-EKF algorithms were utilized for home-on-jam scenarios. Both algorithms performed

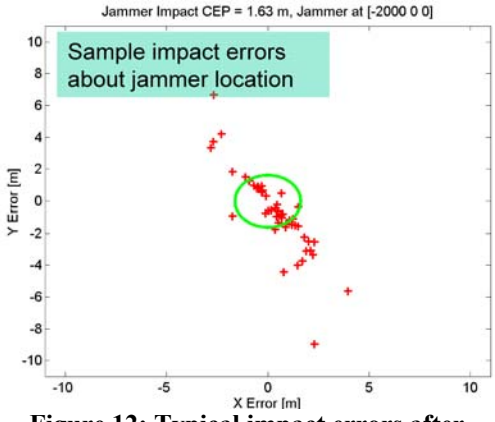

Figure 12: Typical impact errors after homing on the jammer

similarly for stationary jammers while the HC-EKF performed significantly better for moving jammers.

5. CONCLUSIONS

We tested several bearings-only localization algorithms for the purpose of locating GPS jammers from a munition that has lost GPS lock. We found that the HC-EKF performed very well under all scenarios that we considered. While the PLLS filter was stable, it was found to be biased as a function of range, geometry and noise level. The multiple-hypothesis EKF in hybrid-coordinates did not seem to provide any advantages over the single HC-EKF. While the PF errors all did converge to approximately the same values as the HC-EKF, the performance of the HC-EKF algorithms was preferable over the entire munition trajectory and because it is computationally less demanding than the PF.

ACKNOWLEDGMENTS

This research was sponsored in part by the Air Force Research Laboratory (AFRL) under Contracts F08630-00-C-0038 and F08630-01-C-0012. The authors would like to thank George (Eddie) Gibbs, Jr., Capt. Jae Yang, and Capt. Christopher Brann at the Munitions Directorate for their valuable advice and support.

REFERENCES

1. Klotz, H. A. Jr., Derbak, C. B., "GPS-Aided Navigation and Unaided Navigation on the Joint Direct Attack Munition," *IEEE 1998 Position Location and Navigation Symposium*, pp. 412 – 419, 1998.
2. Pace, S., Frost, G., Lachow, I., Frelinger, D., Fossum, D., Wassem, D. K. and Pinto, M., *The Global Positioning System, Assessing National Policies*, RAND, 1995.
3. Aidala, V. J., "Kalman Filter Behavior in Bearings-Only Tracking Applications," *IEEE Transactions on Aerospace and Electronic Systems*, vol. 15, no. 1, January 1979.
4. Nardone, S. C. and Aidala, V. J., "Observability Criteria For Bearings-Only Target Motion Analysis," IEEE Transactions on Aerospace and Electronic Systems, vol. 17, no. 2, March 1981.
5. Hammel, S. E. and Aidala, V. J., "Observability Requirements for Three-Dimensional Tracking via Angle Measurements," *IEEE Transactions on Aerospace and Electronic Systems*, Vol. 21, pp. 200-207, March 1985.
6. Song, T. L. and Speyer, J. L., "A Stochastic Analysis of a Modified Gain Extended Kalman Filter with Applications to Estimation with Bearings Only Measurements," *IEEE Transactions on Automatic Control*, vol. 30, no. 10, October 1985.
7. Lindgren, A. G. and Gong, K. F., "Position and Velocity Estimation Via Bearing Observations," *IEEE Transactions on Aerospace and Electronic Systems*, vol. 14, no. 4, July 1978.
8. Aidala, V. J. and Nardone, S. C., "Biased Estimation Properties of the Pseudolinear Tracking Filter," *IEEE Transactions on Aerospace and Electronic Systems*, vol. 18, no. 4, July 1982.
9. Aidala, V. J. and Hammel, S., "Utilization of Modified Polar Coordinates for Bearings-Only Tracking," *IEEE Transactions on Automatic Controls*, vol. 28, no. 3, March 1983.
10. Grossman, W., "Algebraic Approach to the Bearings-Only Estimation Equations," *Journal of Guidance, Control, and Dynamics*, vol. 14, no. 5, 1991.
11. Grossman, W., "Bearings-Only Tracking: A Hybrid Coordinate System Approach," *Journal of Guidance, Control, and Dynamics*, vol. 17, no. 3, 1994.
12. Peach, N., "Bearings-only tracking using a set of range-parameterized extended Kalman filters," *IEE Proc.-Control Theory Appl.*, vol. 142, no. 1, pp. 73-80, January 1995.
13. Kronhamn, T. R. "Bearings-only target motion analysis based on a multihypothesis Kalman filter and adaptive ownship motion control," IEE Proc.-Radar, Sonar Navig., vol. 145, no. 4, August 1998.
14. Gordon, N. J., Salmond, D. J., and Smith, A. F. M., "Novel Approach to Nonlinear/Non-Gaussian Bayesian State Estimation," IEE Proceedings-F, vol 140, no. 2, pp. 107-113, April 1993.